Journal of Advanced Research 62 (2024) 143–154

Contents lists available at ScienceDirect

Journal of Advanced Research

journal homepage: www.elsevier.com/locate/jare

IFP35 aggravates *Staphylococcus aureus* infection by promoting Nrf2-regulated ferroptosis

Min Dai [a,1], Wei Ouyang [a,1], Yangle Yu [b], Tao Wang [b], Yanling Wang [b], Mengyuan Cen [c], Liping Yang [d], Yu Han [a], Yushi Yao [b], Feng Xu [a,e,*]

[a] Department of Infectious Diseases, The Second Affiliated Hospital, Zhejiang University School of Medicine, Hangzhou 310009, China
[b] Institute of Immunology, Zhejiang University School of Medicine, 310009, China
[c] Department of Respiratory Medicine, Ningbo First Hospital, Ningbo 315010, China
[d] Department of Gastroenterology, Zhejiang Provincial People's Hospital, People's Hospital of Hangzhou Medical College, Hangzhou 310014, China
[e] Research Center for Life Science and Human Health, Binjiang Institute of Zhejiang University, Hangzhou 310053, China

HIGHLIGHTS

- Interferon-induced protein 35 (IFP35) levels increased significantly after *staphylococcus aureus* (SA) infection. IFP35 deficiency protected against SA-induced lung damage in mice.
- Ferroptosis occurred and led to lung injury after SA infection, which was ameliorated by IFP35 deletion.
- IFP35 aggravated SA-induced ferroptosis and tissue injury by enhancing K48-linked ubiquitination and degradation of Nrf2.

GRAPHICAL ABSTRACT

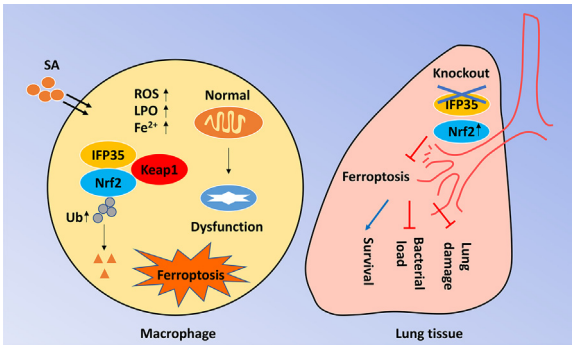

ARTICLE INFO

Article history:
Received 2 April 2023
Revised 26 September 2023
Accepted 27 September 2023
Available online 29 September 2023

Keywords:
Staphylococcus aureus
IFP35
Ferroptosis
NRF2
Ubiquitination

ABSTRACT

Introduction: Serious *Staphylococcus aureus* (SA) infection is one of the most life-threatening diseases. Interferon-induced protein 35 (IFP35) is a pleiotropic factor that participates in multiple biological functions, however, its biological role in SA infection is not fully understood. Ferroptosis is a new type of regulated cell death driven by the accretion of free iron and toxic lipid peroxides and plays critical roles in tissue damage. Whether ferroptosis is involved in SA-induced immunopathology and its regulatory mechanisms remain unknown.
Objectives: We aimed to determine the role and underlying mechanisms of IFP35 in SA-induced lung infections.
Methods: SA infection models were established using wild-type (WT) and IFP35 knockout (*Ifp35*$^{-/-}$) mice or macrophages. Histological analysis was performed to assess lung injury. Quantitative real-time PCR, western blotting, flow cytometry, and confocal microscopy were performed to detect ferroptosis. Co-IP and immunofluorescence were used to elucidate the molecular regulatory mechanisms.
Results: We found that IFP35 levels increased in the macrophages and lung tissue of SA-infected mice.

Abbreviations: IFP35, interferon-induced protein 35; SA, *staphylococcus aureus*; WT, wild-type; ALI, acute lung injury; NMI, N-myc and STAT-interacting protein; BMDMs, bone marrow-derived macrophages; Nrf2, nuclear factor E2 related factor 2; Gpx4, glutathione peroxidase 4; GSH, glutathione; DAMPs, damage associated molecular patterns; MOI, multiplicity of infection; IL-6, interleukin- 6; TNF-α, tumor necrosis factor α; LDH, lactate dehydrogenase; Fer-1, ferrostatin-1; Ptgs2, prostaglandin-endoperoxide synthase 2; ROS, reactive oxygen species; PIH, pyridoxal isonicotinoyl hydrazine; MDA, malondialdehyde; SLC7A11, recombinant solute carrier family 7, Member 11; BALF, bronchoalveolar lavage fluid; CHX, cycloheximide; CHQ, chloroquine; Keap1, kelch-like ECH-associated protein 1; LPO, lipid peroxide; Ub, ubiquitin.

* Corresponding author at: Department of Infectious Diseases, The Second Affiliated Hospital, Zhejiang University School of Medicine, Hangzhou 310009, China.
E-mail address: xufeng99@zju.edu.cn (F. Xu).
[1] Contributed equally.

https://doi.org/10.1016/j.jare.2023.09.042

IFP35 deficiency protected against SA-induced lung damage in mice. Moreover, ferroptosis occurred and contributed to lung injury after SA infection, which was ameliorated by IFP35 deficiency. Mechanically, IFP35 facilitated the ubiquitination and degradation of nuclear factor E2-related factor 2 (Nrf2), aggravating SA-induced ferroptosis and lung injury.

Conclusions: Our data demonstrate that IFP35 promotes ferroptosis by facilitating the ubiquitination and degradation of Nrf2 to exacerbate SA infection. Targeting IFP35 may be a promising approach for treating infectious diseases caused by SA.

Introduction

Staphylococcus aureus (SA) is a gram-positive coccus that can cause life-threatening diseases, such as pneumonia and other infections. The invasion of the lungs by SA significantly contributes to acute lung injury (ALI) and acute respiratory distress syndrome [1]. Although antibiotics can alleviate SA infections, the emergence of new antibiotic-resistant bacterial strains has greatly increased the mortality rate associated with these infections [2]. Hence, besides the development of new antibiotics, alternative and/or adjunctive treatments are urgently needed.

Interferon-induced protein 35 (IFP35) family proteins, including N-myc and STAT-interacting protein (NMI), play vital roles in antivirus responses [3,4]. Moreover, IFP35 and NMI act as damage-associated molecular patterns (DAMPs) that play critical roles in amplifying inflammation. IFP35 deletion alleviated the inflammatory response and increased the survival rate in an LPS-induced sepsis shock mouse model [5]. Several studies have shown that IFP35 is also involved in multiple inflammatory diseases, including sepsis, liver injury, lupus nephritis, and multiple sclerosis [5–8]. A recent study identified IFP35 as a biomarker and therapeutic target in mice infected by SARS-CoV-2 or influenza virus. Neutralizing antibodies against IFP35 significantly reduced lung injury and mortality in infected mice [9]. Although the function of IFP35 in innate immunity is well known, its pathological roles and molecular regulatory mechanisms during bacterial infection, particularly SA infection, remain poorly understood.

Ferroptosis is a novel form of programmed cell death mediated by excessive levels of free iron and lipid peroxides [10]. Ferroptosis is involved in various diseases, including tumors, neurodegenerative diseases, ischemic reperfusion injury, and autoimmune diseases [11–14]. Ferroptotic cell death releases DAMPs and alarm molecules that further amplify the inflammatory response. Ferroptosis is highly immunogenic, thus the inhibition of ferroptosis has significant anti-inflammatory effects [15]. Ferroptosis is closely associated with bacterial infections. *Mycobacterium tuberculosis* can induce ferroptosis in macrophages, which promotes bacterial spread, and exacerbates tissue necrosis [16]. *Pseudomonas aeruginosa* oxidizes arachidonic acid-phosphatidylethanolamine by secreting lipoxygenase to induce ferroptosis in human bronchial epithelial cells [17]. SA induces lipid peroxidation in the lung of cystic fibrosis mice model [18]. In addition, ferrous iron levels increase in SA-stimulated macrophages, which are effective in defending against SA invasion by inducing ferroptosis-like bacterial death [19]. However, whether SA-infected cells undergo ferroptosis is unclear, and if so, the contribution of SA-induced ferroptosis to tissue damage (particularly in lung tissue), remains largely unknown.

Nuclear factor erythroid 2-related factor 2 (Nrf2) is a transcription factor that plays a crucial role in the cellular defence against oxidative stress. Several studies have shown that Nrf2 can regulate ferroptosis in various ways. For example, Nrf2 binds to the antioxidant response element in promoter regions of target genes involved in antioxidant defence, including glutathione peroxidase 4 (GPX4), recombinant solute carrier family 7 member 11 (SLC7A11), heme oxygenase-1 and NAD(P)H quinone oxidoreductase 1. These genes encode proteins that scavenge ROS and detoxify electrophiles [20]. Furthermore, Nrf2 reduces the iron uptake by downregulating the expression of transferrin receptor 1 and divalent metal transporter 1, both of which are involved in iron uptake [21]. Nrf2 activation also enhances glutathione synthesis (GSH) by upregulating the expression of glutamate-cysteine ligase, the rate-limiting enzyme in GSH biosynthesis [22]. Moreover, Nrf2 alleviates ferroptosis-associated ALI and diabetic nephropathy [23–25]. Although the roles of Nrf2 in ferroptosis-mediated pathophysiology have been extensively demonstrated, its roles in SA-mediated immunopathology and the possible mechanisms governing Nrf2 are still largely unknown.

In this study, we found that IFP35 deletion ameliorated lung injury. Furthermore, ferroptosis was induced and contributed to lung injury in mice after SA infection, which was mitigated by IFP35 deficiency. Mechanistically, IFP35 interacted with Nrf2 to promote its ubiquitination and degradation, facilitating SA-induced ferroptosis and lung injury. Our data reveal that IFP35 promotes SA-induced immunopathology in a ferroptosis-related manner, indicating that new treatments for targeting IFP35 or ferroptosis are promising candidates for SA infection.

Materials and methods

Cell culture

Bone marrow–derived macrophages (BMDMs) were established as previously described [26]. BMDMs were cultured in RPMI 1640 - medium (Biological Industries) containing 10 % FBS (Biological Industries), 100 U/mL of penicillin, 100 μg/mL of streptomycin and 20 ng/ml of mouse M-CSF at 37 °C with 5 % CO_2 for 5 days. $CD11b^+F4/80^+$ cells were identified as macrophages. Flow cytometry confirmed that the macrophage purity reached over 90 %. HEK293T cells were originally obtained from American Type Culture Collection. The cells were cultured in DMEM media containing 10 % FBS, 100U/mL of penicillin and 100 μg/mL of streptomycin at 37 °C with 5 % CO_2.

Bacterial culture

SA was cultured aerobically in Tryptic Soy Broth (TSB) medium at 37 °C on a shaking incubator for 14–16 h. Bacteria in logarithmic growth phase were harvested, and washed twice with sterilized PBS by centrifugation at 3000 g for 10 min and finally resuspended in PBS. Growth curves were established by measuring OD600. Bacterial numbers were quantified according to the growth curve and verified with colony-forming unit (CFU) assays.

Quantitative real-time PCR

Total RNA was extracted from cells with an RNA-Quick Purification Kit (ES Science). Then, approximately 200 ng of total mRNA was reverse-transcribed into complementary DNA (cDNA) using PrimeScript™ RT Master Mix (Takara). qRT-PCR was carried out with TB Green® Premix Ex Taq™ (TaKaRa) in the CFX96 Touch Real-Time PCR Detection System (Bio-Rad). After normalizing to internal control (GAPDH) expression, data were determined by the comparative Ct method ($2^{-\Delta\Delta Ct}$). Primer sequences used for qPCR were shown in Supplementary Table 1.

Intracellular ROS, lipid peroxidation and Fe^{2+} detection

5x10^5 BMDMs were plated in a 12-well plate and pretreated with or without the indicated inhibitors, then cells were stimulated with SA at a multiplicity of infection (MOI) of 200 for 3 h. After treatment, cells were incubated with 10 μM of 2′, 7′-dichloro fluorescein-diacetate (DCFH-DA) (Beyotime), 10 μM of LiperFlou (Dojingo) and 1 μM of Ferro orange (Dojingo) for different times according to manuscript instructions respectively. Olympus FV3000 confocal microscope was used to observe and record the results. The excitation and emission wavelengths of DCF (oxidized DCFH-DA by intracellular ROS), oxidized Liperfluo and FerroOrange were 488 and 510 nm, 488 and 510 nm, 561 and 572 nm, respectively.

Ethics statement

All animal experiments were approved by the Animal Care and Use Committee of the Second Affiliated Hospital, Zhejiang University School of Medicine (Approval No. AIRB-2022–091).

Animal experimental design

Ifp35$^{-/-}$ mice (C57BL/6 background) were kindly provided by Dr Ying-Fang Liu (Sun Yat-sen University School of Medicine). *Nrf2*$^{-/-}$ mice were obtained from the ShanghaiModel Organisms and age-matched wild-type C57BL/6 mice were purchased from the Animal Center of Slaccas (Shanghai, China). Female mice were used in experiments. Mice were intraperitoneally injected with ferrostatin-1 (Fer-1) (12.5 μmol/kg) or DMSO solvent control with the same volume and concentration for 1 h prior to infection. Then the mice were anaesthetized by inhalation with 2 % isoflurane and infected intratracheally with SA (1×10^8 CFU) to establish the murine lung infection model. In addition, control ones were administered at equal PBS volume. 24 h later, mice were sacrificed, and samples including bronchoalveolar lavage fluid (BALF) and lung tissue were taken for analysis. For survival study, mice were treated intratracheally with a lethal dose of SA (4×10^8 CFU).

Iron, GSH/GSSG and malondialdehyde (MDA) assays

Lung tissues were washed in cold PBS and homogenized on ice using a Dounce homogenizer, centrifuged at 12000 rpm for 10 min. The supernatants were collected for analysis. Intracellular ferrous iron, GSH/GSSG and MDA were determined using the iron assay kit (Abcam), GSH and GSSG assay kit (Beyotime) and MDA assay kit (Beyotime), respectively. The absorbance at 593, 532 and 412 nm corresponding to iron, GSH/GSSG and MDA levels were determined using a microplate reader (SpectraMax 5).

Histological analysis

The entire lungs of the mice were fixed with 4 % polyformaldehyde overnight at room temperature. Then tissues were embedded in paraffin, cut into 4 μm sections and subjected to hematoxylin and eosin staining. Images were observed using an Olympus BX53 inverted microscope.

Plasmid transfections, immunoblot and immunoprecipitation (IP)

Plasmid transfection was performed using Lipofectamine 3000 (Invitrogen). For some experiments, cells were treated with proteasome inhibitor MG132 (MedChemExpress), protein synthesis inhibitor cycloheximide (CHX) (MedChemExpress) or lysosome inhibitor chloroquine (CHQ) (MedChemExpress) 24–36 h after transfection. Total cell lysates were obtained using WB and IP lysis buffer (Beyotime) supplemented with 1 mM PMSF (Sigma-Aldrich). Immunoblot analysis was performed with indicated antibodies as previously described [27]. For IP, extracts were incubated at 4 °C overnight with anti-Flag M2 magnetic beads or anti-HA magnetic beads. Beads were washed with 1 %-Triton buffer, eluted with 1 × SDS loading buffer, and then operated as immunoblot analysis. The following antibodies were used: GPX4 (Abcam, ab125066), SLC7A11 (Abcam, ab175186), IFP35 (Abnova, H00003430-D01P), Nrf2 (Proteintech, 16396–1-AP), anti-Flag antibody (Beyotime, AF5051), anti-HA antibody (Beyotime, AF2305), anti-Myc antibody (Beyotime, AF2864).

Statistical analysis

Prism 8.0 software (GraphPad, La Jolla, CA, USA) was used for analyzing. Quantitative data were expressed as the means ± SEM. Unpaired student's *t*-test was used for two group comparisons and one-way ANOVA was used for multiple group comparisons. Survival curve analysis was performed using the log rank test. $p < 0.05$ was defined as significant.

Results

IFP35 expression is elevated and its deficiency alleviates lung injury after SA infection

To investigate the potential molecular mechanisms underlying SA infection, we performed a microarray analysis of human monocyte-derived macrophages infected with SA using microarray data from the Gene Expression Omnibus (GEO). We found that the mRNA expression of IFP35 was significantly increased in SA-infected macrophages (GEO dataset, GDS4931) (Fig. 1a). Furthermore, we observed increased IFP35 staining intensity levels in lung tissue of SA-infected mice (Fig. 1b). Upregulated IFP35 mRNA and protein levels were also confirmed in BMDMs infected with SA (Fig. 1c-d). To clarify the role of IFP35 in SA infection, WT and *Ifp35*$^{-/-}$ mice were intratracheally injected with a lethal dose of SA, and the *Ifp35*$^{-/-}$ mice showed a higher survival rate (Fig. 1e). Moreover, a lower expression of interleukin-6 (IL-6) and tumor necrosis factor α (TNF-α) in the BALF and a lower bacterial load in lung tissue of *Ifp35*$^{-/-}$ mice were observed (Fig. 1f-h). Similarly, significant attenuation of lung injury was observed in *Ifp35*$^{-/-}$ mice compared to that in WT mice after SA infection, according to the histological analysis (Fig. 1i). These results suggested that IFP35 aggravated SA infection *in vivo*.

Ferroptosis occurred in vivo and in vitro after SA infection

Recent studies have found that ferroptosis has a significant effect on bacterial infection. Upon infection with SA, ferrous iron and lipid peroxidation levels increase in macrophages, suggesting the possible occurrence of ferroptosis [18,19]. Therefore, we infected mice and BMDMs with SA and performed a series of

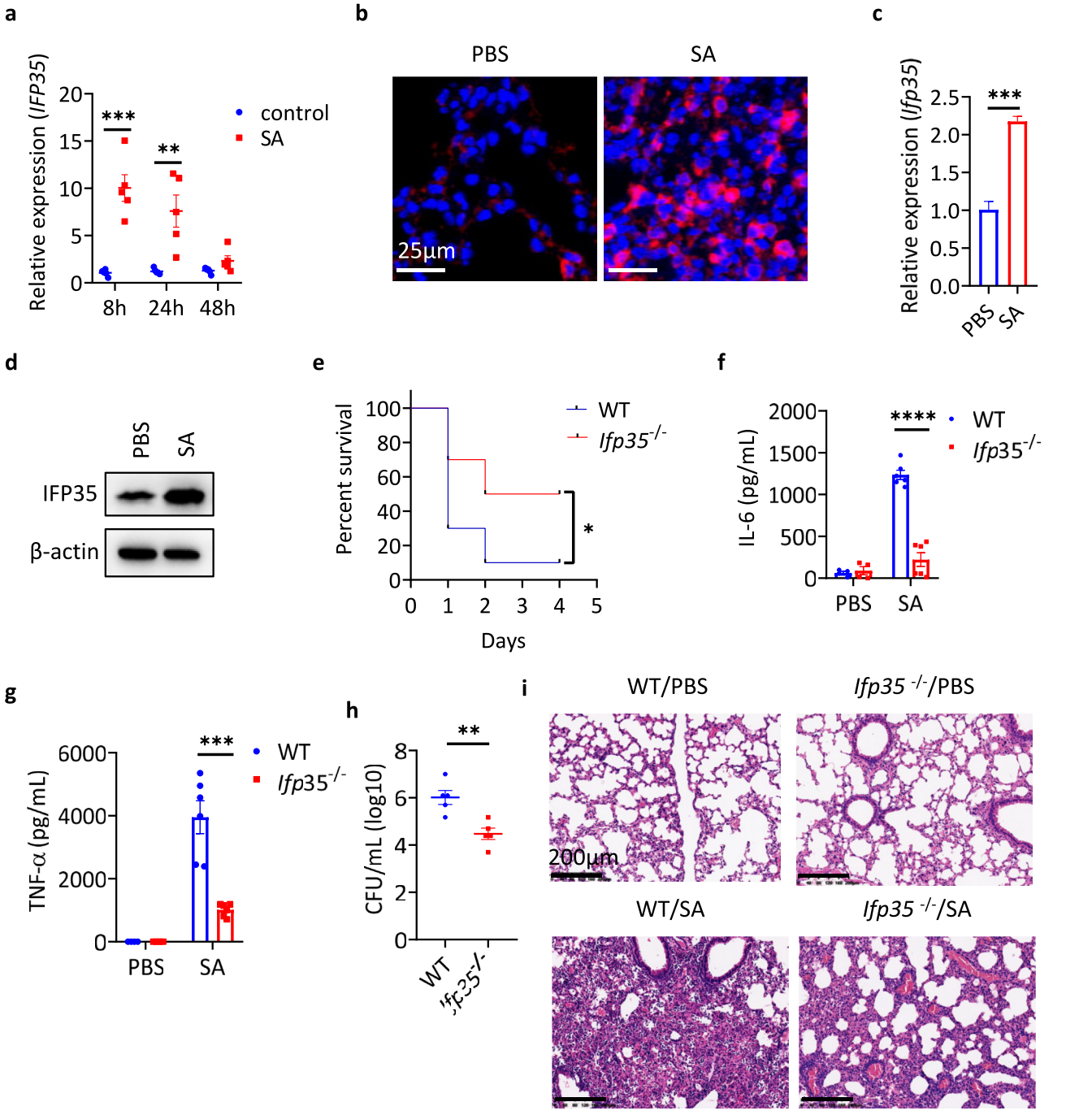

Fig 1. IFP35 expression is elevated and its deficiency alleviates lung injury after SA infection. (a) Expression of IFP35 in monocyte-derived human macrophages that phagocytosed SA *in vitro* was analyzed. The raw data (GDS4931) derived from Gene Expression Omnibus datasets. (b) Mice were *i.t.* with a sublethal dose (1×10^8 CFU, n = 3 mice/group) of SA for 24 h. IFP35 staining intensity levels in lung tissue were assessed. (c-d) BMDMs were infected with SA (MOI = 200) for 4 h, the gene and protein levels of IFP35 were detected. (e) WT and *Ifp35*$^{-/-}$ mice were *i.t.* with a lethal dose (4×10^8 CFU, n = 10 mice/group) of SA for 5 days, mice survival rate was observed. (f-i) WT and *Ifp35*$^{-/-}$ mice were *i.t.* with a sublethal dose (1×10^8 CFU, n = 4–6 mice/group) of SA for 24 h. (f-g) Concentrations of IL-6 and TNF-α levels in the BALF were measured. (h) Pulmonary bacterial load in lung tissue was determined. (i) Representative H&E staining images of merged lung sections were observed. (scale bars, 200 μm). Data in bar graphs and scattered dot plots are presented as mean ± SEM, $^*p < 0.05$; $^{**}p < 0.01$; $^{***}p < 0.001$; $^{****}p < 0.0001$.

experiments to evaluate ferroptosis at organ and cellular levels. As expected, higher iron levels were detected in lung tissue of infected mice than in those of uninfected mice (Fig. 2a). The changes in the redox status and in the levels of malondialdehyde (MDA), a major lipid peroxidation product, were assessed. Decreased GSH/GSSG ratios (Fig. 2b) and increased MDA levels (Fig. 2c) were observed in lung tissue after SA infection. Furthermore, the protein levels of ferroptosis-related molecules, including GPX4 and SLC7A11, were decreased (Fig. 2d) in lung tissue of infected mice. Notably, these ferroptosis-related changes in infected mice were significantly inhibited by ferostatin-1 (Fer-1), a well-characterized ferroptosis inhibitor, suggesting that ferroptosis is involved in SA-induced pulmonary infections. Monocytes/macrophages and neutrophils are vital inflammatory cells in the alveoli after SA infection, where ferroptosis may occur and affect pathogenesis. We found that SA infection triggered an increase in both the levels of

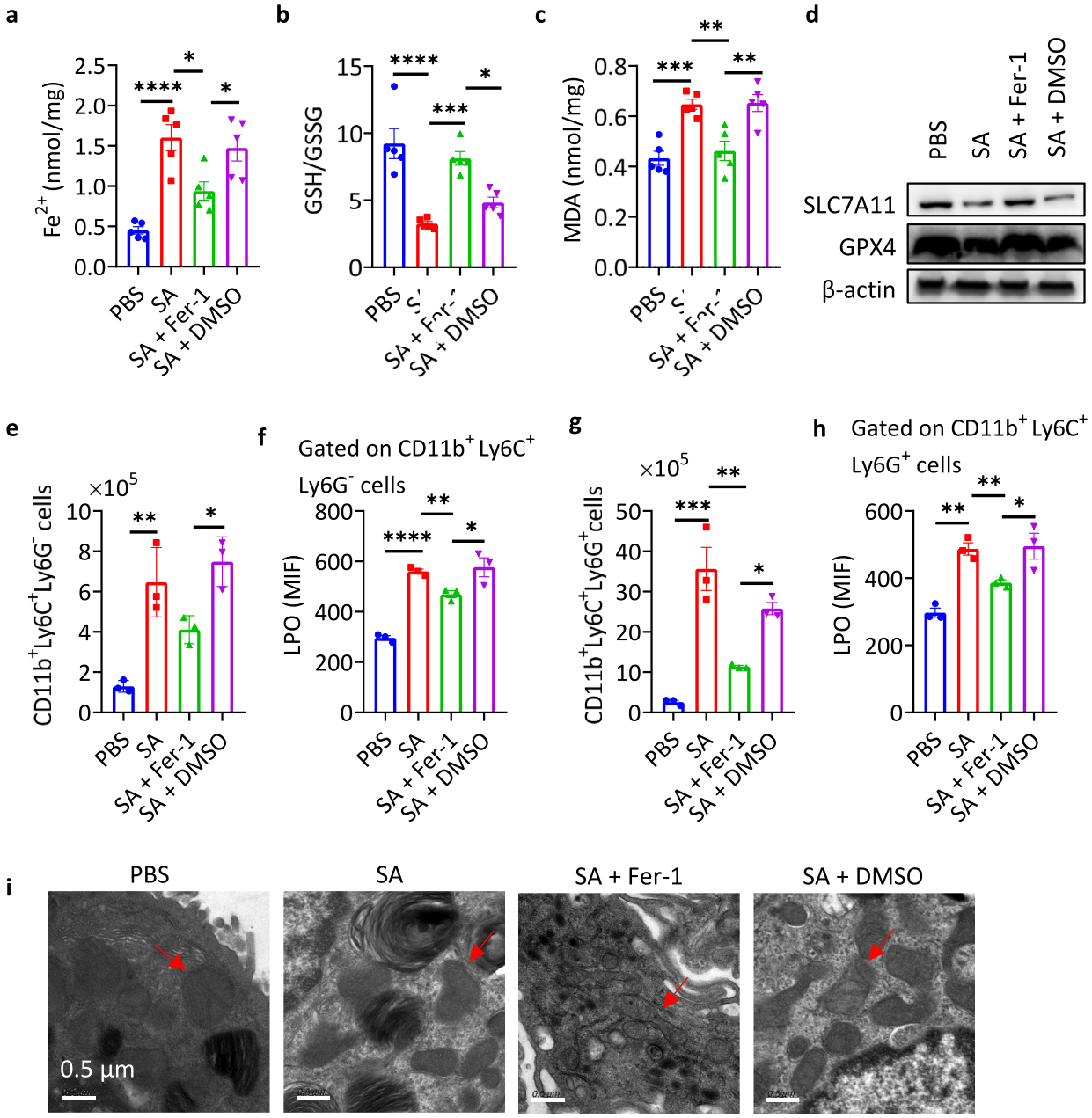

Fig 2. Ferroptosis occurred in lung tissues of SA-infected mice. WT mice were *i.p.* with the same volume of Fer-1 or DMSO at the same concentration (12.5 μmol/kg), and 1 h later, *i.t.* with a sublethal dose (1×10^8 CFU, n = 3–5 mice/group) of SA. Lung tissues were harvested at 24 h post-infection. (a-c) Concentrations of iron, GSH/GSSG, and MDA were detected. (d) GPX4 and SLC7A11 proteins levels were determined. (e) The numbers of $CD45^+CD11b^+Ly6C^+Ly6G^-$ monocytes/macrophages were counted. (f) LPO levels in $CD45^+CD11b^+Ly6C^+Ly6G^-$ monocytes/macrophages were analyzed. (g) The numbers of $CD45^+CD11b^+Ly6C^+Ly6G^+$ neutrophils were counted. (h) LPO levels in $CD45^+CD11b^+Ly6C^+Ly6G^+$ neutrophil subsets were analyzed. (i) The mitochondrial morphology of mouse lung tissue was observed. (scale bars, 0.5 μm). Data in scattered dot plots are presented as mean ± SEM, $^*p < 0.05$; $^{**}p < 0.01$; $^{***}p < 0.001$; $^{****}p < 0.0001$.

$CD11b^+Ly6C^+Ly6G^-$ monocytes/macrophages and $CD11b^+Ly6C^+$-$Ly6G^+$ neutrophils, as well as in their lipid peroxidation levels. These alterations were suppressed by pretreating the infected mice with Fer-1 (Fig. 2e-h). Finally, fewer mitochondrial cristae were observed in lung tissue after SA infection, which represents a remarkable morphological change occurring during ferroptosis (Fig. 2i). These results suggested that SA induced ferroptosis in lung tissue of mice.

Next, we examined the *in vitro* SA-induced cell death by infecting BMDMs with SA at different MOIs. Cell death was assessed by detecting the release of lactate dehydrogenase (LDH) into the cell supernatants. The cell death of the BMDMs infected with SA increased in an MOI-dependent manner (Fig. S1a). To investigate whether SA induced cell death via ferroptosis, the cells were pretreated with different concentrations of Fer-1. Fer-1 could partially inhibit cell death at a concentration of 10 μM (Fig. S1b). A remarkable decrease in *Gpx4*expression and an increase in prostaglandin-endoperoxide synthase (*Ptgs2*) expression were observed in BMDMs infected with SA (Fig. S1c-d). In addition, the levels of ferroptosis hallmarks, including ROS, lipid peroxide, and free iron, increased after SA infection, as shown by the intracellular staining results (Fig. S1e). Notably, these ferroptosis-related changes were partially abrogated by the pretreatment of BMDMs with Fer-1 (Fig. S1c-e). Transmission electron microscopy results revealed that the mitochondria in SA-infected BMDMs showed key ferroptosis features, including shrunken mitochondria, an increased mem-

brane density, and reduced or even lost mitochondrial cristae. As expected, pretreatment with Fer-1 significantly reduced mitochondrial damage in SA-infected BMDMs (Fig. S1f). To determine whether SA-induced cell death was iron-dependent, we pretreated the BMDMs with pyridoxal isonicotinoyl hydrazone (PIH), an iron chelator, which resulted in reduced cell death (Fig. S1g) and *Ptgs2* expression (Fig. S1h). Collectively, these observations suggested that SA triggers ferroptosis in macrophages.

Inhibition of ferroptosis reduces the bacterial load and alleviates pulmonary pathological changes in SA-infected mice

Ferroptosis is a form of programmed cell death with strong immunogenicity and is considered as a target for therapeutic intervention in several inflammatory diseases [28]**.** Next, we determined the effect of ferroptosis inhibition on SA-induced lung inflammation and injury. The mice were intraperitoneally administered with Fer-1 (12.5 μmol/kg) 1 h before SA infection. Our data showed that the survival rate of the mice pretreated with Fer-1 increased (Fig. 3a). Pretreatment with Fer-1 also reduced the levels of pro-inflammatory cytokines, including IL-6 and TNF-α, in the BALF of SA-infected mice (Fig. 3b-c). Furthermore, ferroptosis inhibition decreased the bacterial load in SA-infected lung tissues (Fig. 3d). Pulmonary histopathological examination confirmed that pretreatment with Fer-1 relieved SA-induced lung injury, including interstitial congestion and edema, alveolar septal thickening, and infiltration of inflammatory cells into lung parenchyma and alveolar spaces (Fig. 3e).

Effect of IFP35 deletion on SA-induced ferroptosis in vivo and in vitro

As shown above, SA induced cell death and pulmonary immunopathology through ferroptosis. We questioned whether the protective effects of IFP35 deficiency on SA infection could be attributed to reduced ferroptosis. We challenged *Ifp35*$^{-/-}$ and WT mice with SA. As expected, *Ifp35*$^{-/-}$ mice showed lower iron levels (Fig. 4a), higher GSH/GSSG ratios (Fig. 4b), and lower MDA levels (Fig. 4c) in lung tissue compared with WT mice. Moreover, pulmonary GPX4 and SLC7A11 protein levels were significantly higher in *Ifp35*$^{-/-}$ mice after SA infection (Fig. 4d). In addition, the number of CD11b^{+}Ly6C^{+}Ly6G^{-} monocytes/macrophages and CD11b^{+}Ly6C^{+}-Ly6G^{+} neutrophils decreased, as did their lipid peroxidation levels, in SA-infected *Ifp35*$^{-/-}$ mice (Fig. 4e-h). These data favored a protective role for IFP35 deletion against SA-induced ferroptosis in lung tissue.

Next, we assessed the effect of IFP35 deficiency on SA-induced ferroptosis *in vitro*. WT and IFP35-knockout BMDMs were infected with bacteria at different MOIs. Data showed that cell death of IFP35-knockout cells at an MOI of 100 or 200 was lower than that of WT cells (Fig. 4i). In addition, increased *Gpx4* expression and decreased *Ptgs2* expression were observed in IFP35-deficient BMDMs (Fig. 4j-k). Intracellular staining showed that IFP35 deficiency reduced levels of key ferroptosis-related markers, including intracellular ROS, lipid peroxides, and iron, after SA infection (Fig. 4l). Collectively, these data demonstrated that IFP35 deficiency ameliorated SA-induced ferroptosis in macrophages.

IFP35 deficiency inhibits ferroptosis through an Nrf2-dependent mechanism

Next, we explored the molecular mechanism by which IFP35 knockout reduced SA-mediated ferroptosis. As shown above, IFP35 deletion enhanced GPX4 and SLC7A11 expression and reduced ROS, lipid peroxides, and iron levels in SA-infected BMDMs. Given the different ways in which Nrf2 regulates ferroptosis, we questioned whether IFP35 regulates SA-mediated ferroptosis via Nrf2. IFP35-knockout and WT cells were infected with SA, and we found that the *Nrf2* mRNA levels of IFP35-knockout and WT BMDMs did not differ (Fig. 5a); however, the protein levels of IFP35-knockout BMDMs were higher than those of WT BMDMs after SA stimulation (Fig. 5b). To investigate the role of Nrf2 in SA-induced ferroptosis, we treated the BMDMs from WT and *Nrf2*$^{-/-}$ mice with SA at various MOIs. As expected, the cell death of Nrf2-knockout BMDMs was higher when the cells were infected at an MOI of 100 and 200. This was completely reversed by Fer-1 pretreatment (Fig. 5c). *Gpx4* expression decreased and *Ptgs2* expression increased in Nrf2-deficient cells following SA infection (Fig. 5d-e). In addition, increased intracellular ROS, lipid peroxides, and iron levels, were observed in SA-treated Nrf2-deficient cells using a confocal microscope (Fig. 5f). The changes in all these ferroptosis-related indicators were also significantly reversed via Fer-1 pretreatment. These findings demonstrated that Nrf2 played an important role in resistance to SA-induced ferroptosis in macrophages. To further clarify whether IFP35 deficiency ameliorates ferroptosis by upregulating Nrf2, we pretreated IFP35-knockout cells with brusatol, a Nrf2-specific inhibitor. Nrf2 inhibition significantly increased cell death and *Ptgs2* expression in IFP35-knockout BMDMs, to levels even higher than those of WT cells (Fig. 5g-h). Confocal microscopy revealed that Nrf2 suppression significantly increased ROS, lipid peroxides, and iron levels of IFP35-knockout cells (Fig. 5i). Taken together, these data indicated that IFP35 deficiency ameliorated ferroptosis by upregulating Nrf2 expression.

IFP35 promotes Nrf2 degradation via K48-linked ubiquitination

Under homeostatic conditions, Nrf2 is rapidly ubiquitinated and degraded by binding to Kelch-like ECH-associated protein 1 (Keap1) in the cytoplasm. Upon exposure to oxidative stress, Nrf2 is activated and separated from Keap1. Activated Nrf2 translocates to the nucleus to promote transcription of antioxidant genes [29]. Considering that IFP35 decreased Nrf2 protein expression but had no effect on the mRNA level, we hypothesized that IFP35 enhanced the degradation of Nrf2. To test this hypothesis, we examined the interaction between IFP35 and Nrf2 in cells. Under confocal microscopy, an enhanced co-localization of IFP35 and Nrf2 was found in SA-infected BMDMs and 293 T cells compared to that of uninfected cells (Fig. 6a-b). The interaction between IFP35 and Nrf2 was also confirmed by co-immunoprecipitation and immunoblot analyses of transfected 293 T cells (Fig. 6c-d). Next, we investigated whether IFP35 promoted Nrf2 degradation by treating cells with a protein synthesis inhibitor (cycloheximide, (CHX)) at different time points. Immunoblot analysis showed that IFP35 enhanced Nrf2 degradation in a time and dose-dependent manner (Fig. 6e-f), and this effect was reversed by treatment with the proteasome inhibitor MG132 rather than with the lysosome inhibitor (chloroquine, (CHQ)) (Fig. 6g). These results suggested that IFP35 promoted Nrf2 degradation through the ubiquitin–proteasome pathway. Ubiquitination is an important step in the proteasome-mediated protein degradation [30]. We examined the effect of IFP35 on Nrf2 ubiquitination and found that IFP35 overexpression increased Nrf2 ubiquitination (Fig. 6h). Lysine 48 (-K48)-linked ubiquitination is required for proteasomal degradation. Thus, we tested the effect of IFP35 on the K48-linked ubiquitination of Nrf2, and observed that IFP35 overexpression increased this parameter (Fig. 6i). Considering the critical role of Keap1 in Nrf2 degradation, we investigated the effect of IFP35 on Keap1 level. Interestingly, IFP35 also interacted with Keap1 in 293 T cells and that IFP35 overexpression increased Keap1 protein levels (Fig. 6j-l), indicating that IFP35 can also promote Nrf2 degradation by regulating the Keap1 level. Collectively, these data demonstrated that IFP35 interacted with Nrf2 and Keap1 and pro-

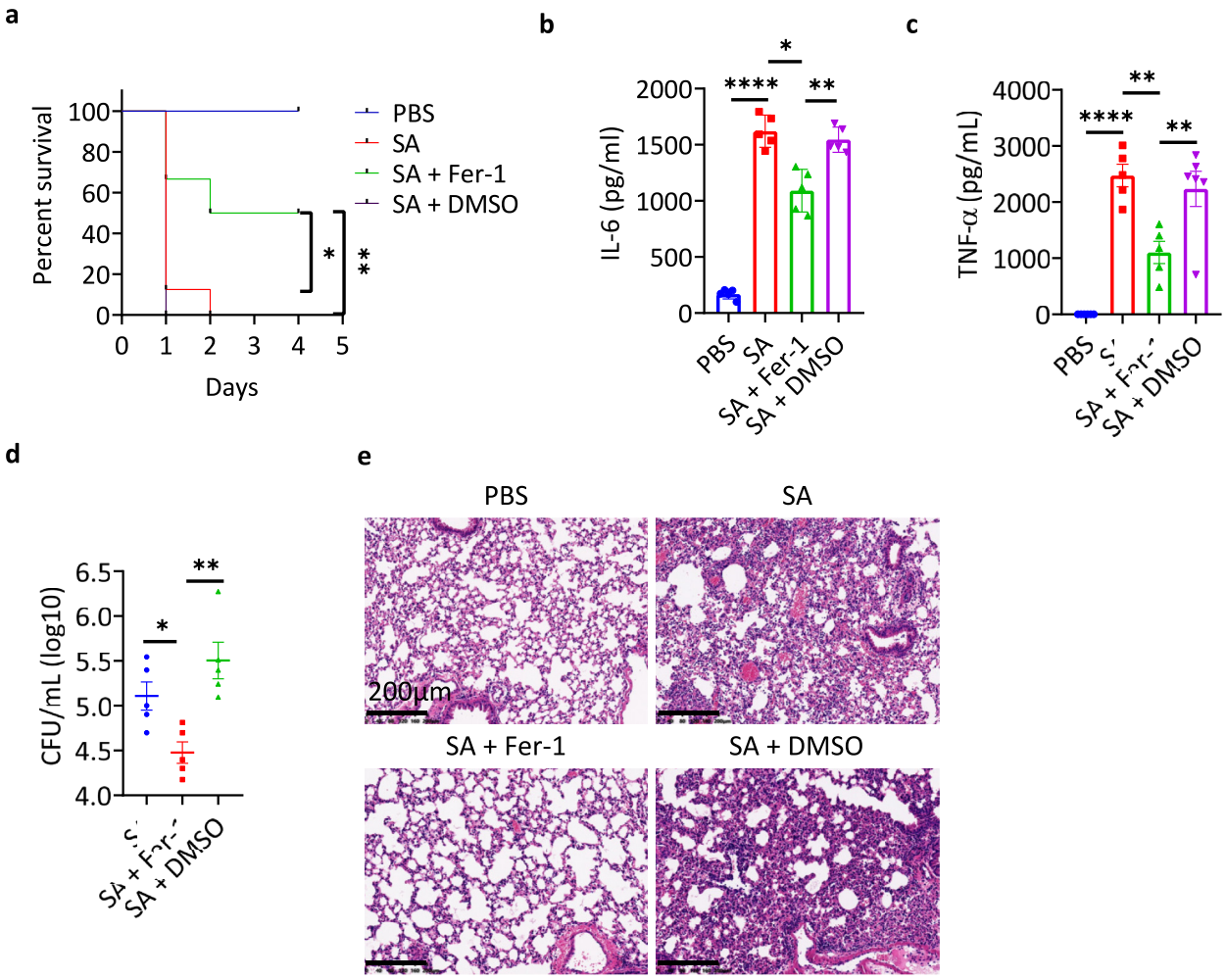

Fig 3. Ferroptosis inhibition reduces the bacterial load and alleviates pulmonary pathological changes in SA-infected mice. (a) WT mice were *i.t.* with a lethal dose (4×10^8 CFU, n = 6–8 mice/group) of SA for 5 days after being *i.p.* with the same volume of Fer-1 or DMSO at the same concentration (12.5 μmol/kg), 1 h earlier, mice survival rate was observed. (b-e) WT mice were *i.t.* with a sublethal dose (1×10^8 CFU, n = 5–6 mice/group) of SA for 24 h after being *i.p.* with Fer-1 or DMSO (12.5 μmol/kg), 1 h earlier. (b-c) Concentrations of IL-6 and TNF-α levels in the BALF were detected. (d) Pulmonary bacterial loads were measured. (e) Representative H&E staining images of the merged lung sections were observed. (scale bars, 200 μm). Data in scattered dot plots are presented as mean ± SEM, $^*p < 0.05$; $^{**}p < 0.01$; $^{****}p < 0.0001$.

moted K48-linked ubiquitination and degradation of Nrf2 via the proteasome pathway.

Discussion

Our major findings demonstrated that IFP35 aggravated SA induced lung injury. Ferroptosis occurred and contributed to SA-induced tissue damage. IFP35 promoted SA-induced ferroptosis by modulating Nrf2 stability to facilitate the pathological processes. The serum IFP35 concentration is highly correlated with COVID-19 severity. Additionally, the administration of an anti-IFP35 neutralizing antibody significantly reduced lung injury and mortality in SARS-COVID-2- and influenza-infected mice [9]. Here, we showed for the first time that IFP35 expression increased significantly after SA infection. Our results suggested that *Ifp35*$^{-/-}$ mice exhibited increased survival, reduced bacterial load, and less lung injury, supporting the essential role of IFP35 deficiency in alleviating inflammation and lung injury. IFP35 can promote apoptosis and ROS production to inhibit tumorigenesis [31]. Furthermore, IFP35 promotes tumour growth and lung metastasis during renal cancer progression by inhibiting autophagy induction [32]. Here, IFP35 was functionally significant in executing SA-induced ferroptosis, as IFP35 deficiency ameliorated SA-induced ROS production, lipid peroxidation, and iron accumulation. These findings confirm the crucial role of IFP35 in facilitating SA-induced lung injury by promoting ferroptosis.

Ferroptosis is a form of programmed cell death that is triggered by iron-dependent lipid peroxidation, resulting in plasma membrane damage. In recent years, emerging reports have suggested that ferroptosis is activated during bacterial infection-related injury in host tissues [33]. In this study, we experimentally demonstrated that ferroptosis was activated after SA infection. Elevated levels of ROS, lipid peroxides, and free iron were detected in SA-infected cells and lung tissues, whereas these effects of SA infection were abrogated by Fer-1. In addition, the lethality, inflammatory response, and lung injury were partially reversed by Fer-1 pretreatment in SA-infected mice. These results indicate that ferroptosis is a potential therapeutic intervention target. Nevertheless, considering that ferroptosis inhibition did not completely block SA-mediated cell death effects, our findings cannot formally exclude intersections with other cell death pathways, such as pyroptosis and necroptosis [34,35].

Nrf2 is a critical cytoprotective factor that regulates antioxidant responses by controlling the expression of genes that eliminate oxidative and electrophilic stresses [36]. It is well established that Nrf2 plays a positive role in reducing iron and ROS levels. Nrf2 tar-

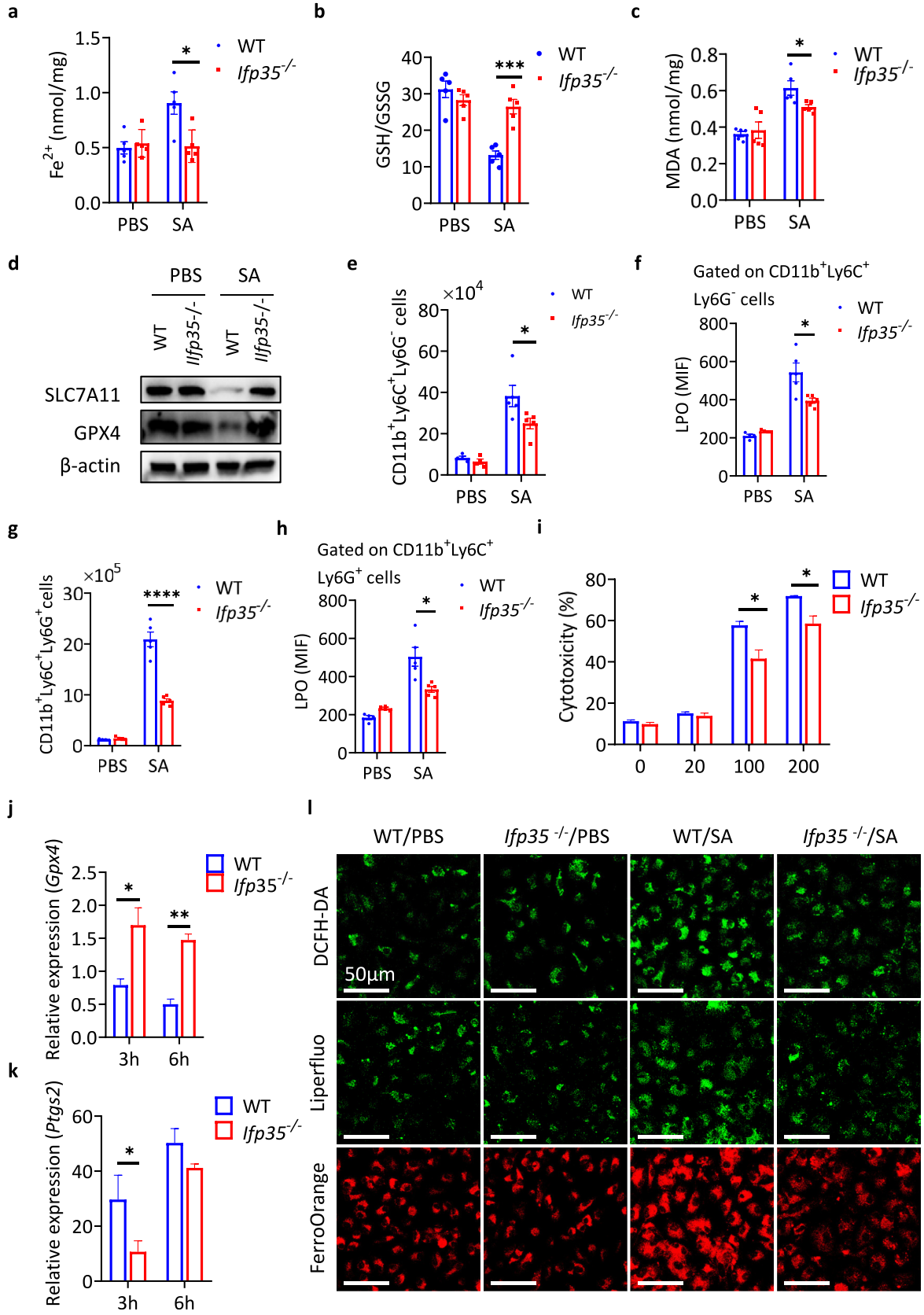

Fig 4. Effect of IFP35 deletion on SA-induced ferroptosis*in vivo* and *in vitro*. WT and *Ifp35*$^{-/-}$ mice were *i.t.* with a sublethal dose (1×10^8 CFU, n = 4–5 mice/group) of SA. Lung tissues were harvested at 24 h post-infection. (a-c) Concentration of iron, GSH/GSSG, and MDA were detected. (d) Levels of GPX4 and SLC7A11 proteins were determined. (e) The numbers of CD45$^+$CD11b$^+$Ly6C$^+$Ly6G$^-$ monocytes/macrophages were counted. (f) LPO levels in CD45$^+$CD11b$^+$Ly6C$^+$Ly6G$^-$ monocytes/macrophages were analyzed. (g) The numbers of CD45$^+$CD11b$^+$Ly6C$^+$Ly6G$^+$ neutrophils were counted. (h) LPO levels in CD45$^+$CD11b$^+$Ly6C$^+$Ly6G$^+$ neutrophil subsets were analyzed. (i) WT and IFP35-deficient BMDMs were infected with SA at different MOIs, cytotoxicity was assessed. (j-k) WT and IFP35-deficient BMDMs were infected with SA (MOI = 200) for 4 h, *Gpx4* and *Ptgs2* mRNA expression levels were detected. (l) WT and IFP35-deficient BMDMs were infected with SA (MOI = 200) for 3 h, representative fluorescence images showed the production of ROS, LPO, and Fe^{2+}. DCFH-DA staining represented intracellular ROS, Liperfluo staining represented LPO, and FerroOrange staining represented intracellular Fe^{2+}. (scale bars, 50 μm). Data in bar graphs and scattered dot plots are presented as mean ± SEM, *$p < 0.05$; **$p < 0.01$; ***$p < 0.001$; ****$p < 0.0001$.

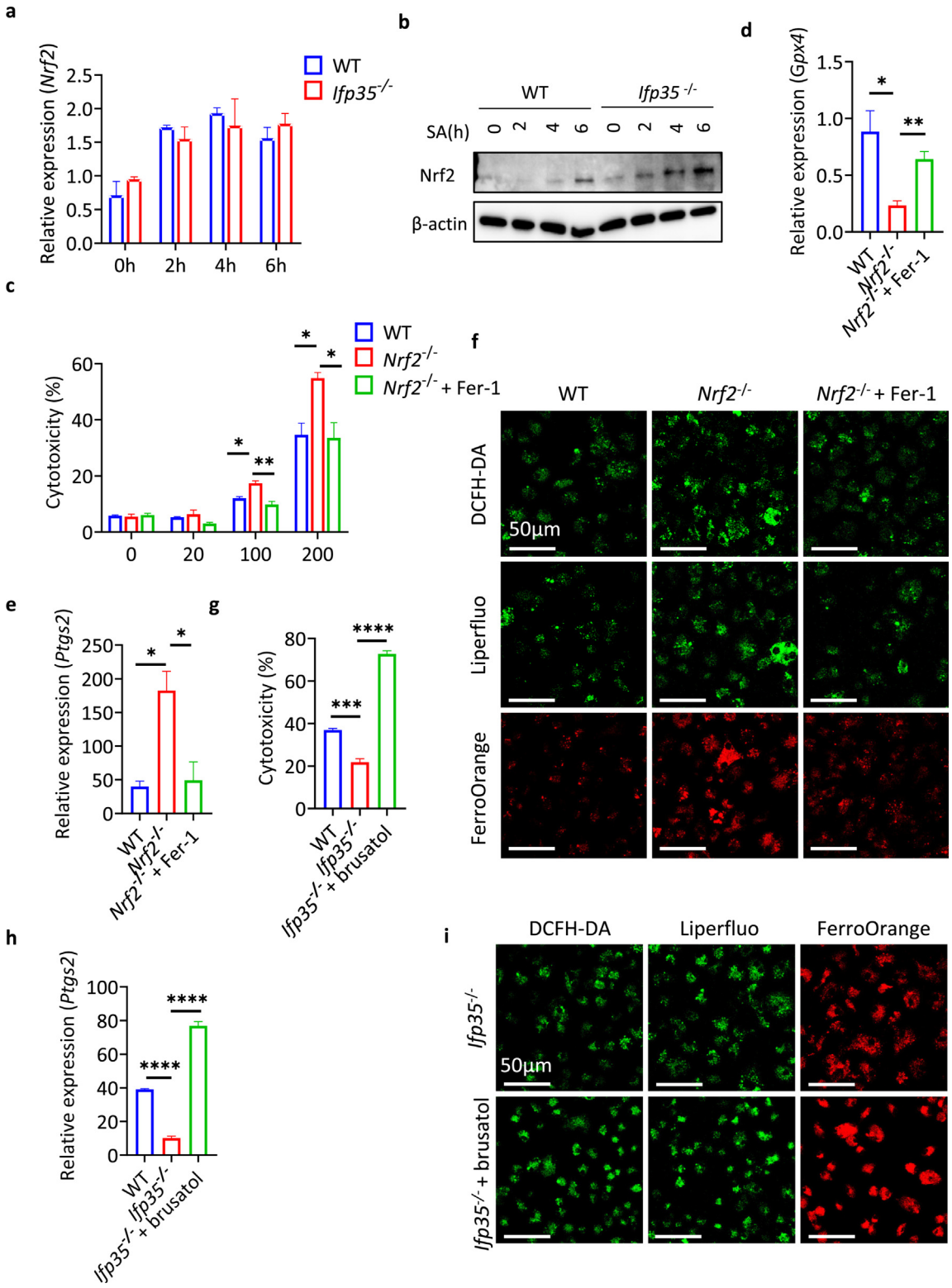

Fig 5. IFP35 deficiency inhibits ferroptosis through an Nrf2-dependent mechanism. (a-b) WT and IFP35-deficient BMDMs were infected with SA (MOI = 200) at different time points, Nrf2 mRNA and protein levels were detected. (c) WT and Nrf2-deficient BMDMs were pretreated with Fer-1 or not and infected with SA at different MOIs, cytotoxicity was assessed. (d-e) WT and Nrf2-deficient BMDMs were pretreated with Fer-1 or not and infected with SA (MOI = 200) for 4 h, *Gpx4* and *Ptgs2* mRNA expression levels were detected. (f) WT and Nrf2-deficient BMDMs were pretreated with Fer-1 or not and infected with SA (MOI = 200) for 3 h, representative fluorescence images showed the production of ROS, LPO, and Fe^{2+}. DCFH-DA staining represented intracellular ROS, Liperfluo staining represented LPO, and FerroOrange staining represented intracellular Fe^{2+}. (scale bars, 50 μm). (g-h) WT and IFP35-deficient BMDMs were infected with SA (MOI = 200) for 4 h after pretreatment with or without brusatol (40 nM) 1 h earlier. (g) Cytotoxicity was determined. (h) *Ptgs2* mRNA expression levels were measured. (i) WT and IFP35-deficient BMDMs were infected with SA (MOI = 200) for 3 h after pretreatment with or without brusatol (40 nM) 1 h earlier, representative fluorescence images showed the production of ROS, LPO, and Fe^{2+}. DCFH-DA staining represented intracellular ROS, Liperfluo staining represented LPO, and FerroOrange staining represented intracellular Fe^{2+}. (scale bars, 50 μm). Data in bar graphs are presented as mean ± SEM, $^{*}p < 0.05$; $^{**}p < 0.01$; $^{***}p < 0.001$; $^{****}p < 0.0001$.

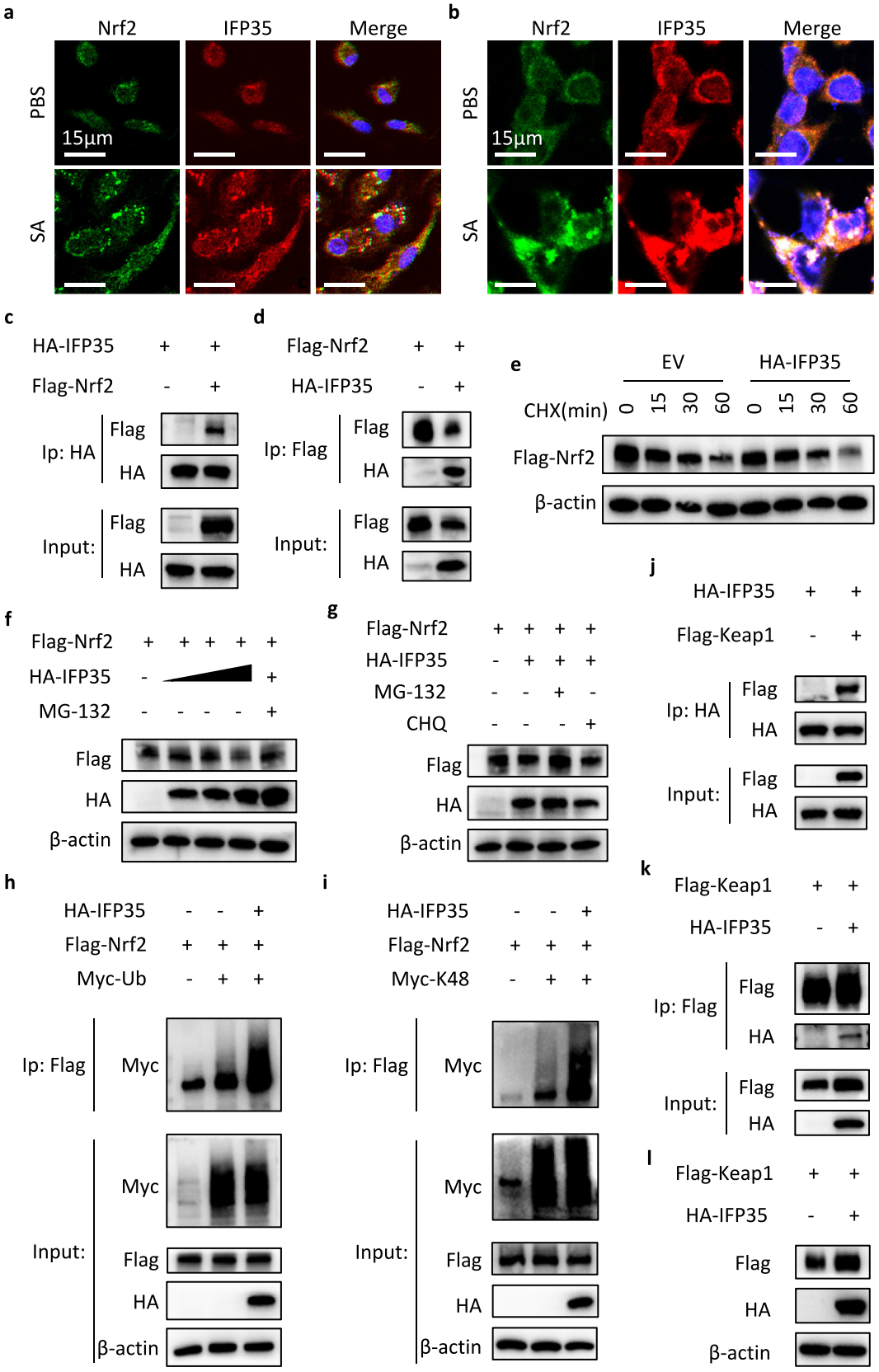
a
Nrf2
IFP35
Merge
PBS
SA
15μm
b
Nrf2
IFP35
Merge
PBS
SA
15μm
c
HA-IFP35 + +
Flag-Nrf2 - +
Ip: HA
Flag
HA
Input:
Flag
HA
d
Flag-Nrf2 + +
HA-IFP35 - +
Ip: Flag
Flag
HA
Input:
Flag
HA
e
EV
HA-IFP35
CHX(min) 0 15 30 60 0 15 30 60
Flag-Nrf2
β-actin
f
Flag-Nrf2 + + + + +
HA-IFP35 - +
MG-132 - - - - +
Flag
HA
β-actin
g
Flag-Nrf2 + + + +
HA-IFP35 - + + +
MG-132 - - + -
CHQ - - - +
Flag
HA
β-actin
h
HA-IFP35 - - +
Flag-Nrf2 + + +
Myc-Ub - + +
Ip: Flag
Myc
Input:
Myc
Flag
HA
β-actin
i
HA-IFP35 - - +
Flag-Nrf2 + + +
Myc-K48 - + +
Ip: Flag
Myc
Input:
Myc
Flag
HA
β-actin
j
HA-IFP35 + +
Flag-Keap1 - +
Ip: HA
Flag
HA
Input:
Flag
HA
k
Flag-Keap1 + +
HA-IFP35 - +
Ip: Flag
Flag
HA
Input:
Flag
HA
l
Flag-Keap1 + +
HA-IFP35 - +
Flag
HA
β-actin

gets several genes that mitigate lipid peroxide formation and ferroptotic cascade [37]. Here, we showed that Nrf2-deficient cells exhibited increased ferroptotic cell death. We also found an increased Nrf2 protein level in IFP35-knockout cells. Nrf2 inhibition significantly enhanced ferroptosis and *Ptgs2* expression in IFP35-knockout cells. Our data demonstrated that IFP35-deficient cells inhibited ferroptosis by upregulating Nrf2. Under unstressed conditions, Keap1 binds to Nrf2 in the cytoplasm and promotes its proteasomal degradation [29]. E3 ubiquitin ligase complexes control ubiquitination and proteasomal degradation of Nrf2 [38]. Intracellular IFP35 mediates the ubiquitination of RIG-I, which is involved in innate immunity [39]. Our data showed that IFP35 interacted with Nrf2 and Keap1, promoting the K48-linked ubiquitination and degradation of Nrf2 through the proteasome pathway. Given the numerous ways in which Nrf2 promotes cell survival, it is not surprising that blocking Nrf2 or its downstream targets can reduce the ability of cells to respond to stress and lead to increased cell death, such as pyroptosis and ferroptosis. Although our study focused on the involvement of Nrf2 in SA-induced ferroptosis, we need to further explore the possibility that pyroptosis is involved in this process.

Conclusion

In summary, our study suggested the deleterious effects of IFP35 on immunopathology evoked by SA infection. Ferroptosis was involved in SA-induced pathological processes, and IFP35 deletion reduced SA-mediated ferroptosis. Mechanistic investigations indicated that IFP35 deficiency upregulated Nrf2 by inhibiting its ubiquitination and degradation to reduce the ferroptosis induced by SA. Our study provides novel insights into the pathogenesis of SA infections. The specific targeting of IFP35, or ferroptosis, is a promising strategy for the treatment of diseases associated with SA.

Compliance with Ethics Requirements

All Institutional and National Guidelines for the care and use of animals (fisheries) were followed.

Declaration of Competing Interest

The authors declare that they have no known competing financial interests or personal relationships that could have appeared to influence the work reported in this paper.

Acknowledgements

This work was supported by National Natural Science Foundation of China (No. 82241046 and 81970004), Natural Science Foundation of Zhejiang Province (LQ23H010004), Binjiang Institute of Zhejiang University (ZY202205SMKY006), and Qianjiang Distinguished Scholar Program from Hangzhou City. We thank the Core Facilities of Zhejiang University of Medicine for technical assistance. We thank the Laboratory Animal Center of Zhejiang University for mice breeding.

Appendix A. Supplementary data

Supplementary data to this article can be found online at https://doi.org/10.1016/j.jare.2023.09.042.

References

[1] Chastre J, Trouillet JL, Vuagnat A, et al. Nosocomial pneumonia in patients with acute respiratory distress syndrome. Am J Respir Crit Care Med 1998;157(4 Pt 1):1165–72. doi: https://doi.org/10.1164/ajrccm.157.4.9708057.
[2] Ogundipe FO, Ojo OE, Feßler AT, et al. Antimicrobial Resistance and Virulence of Methicillin-Resistant *Staphylococcus aureus* from Human, Chicken and Environmental Samples within Live Bird Markets in Three Nigerian Cities. Antibiotics (Basel) 2020. 9(9).10.3390/antibiotics9090588.
[3] Tan J, Qiao W, Wang J, et al. IFP35 is involved in the antiviral function of interferon by association with the viral tas transactivator of bovine foamy virus. J Virol 2008;82(9):4275–83. doi: https://doi.org/10.1128/jvi.02249-07.
[4] Gounder AP, Yokoyama CC, Jarjour NN, et al. Interferon induced protein 35 exacerbates H5N1 influenza disease through the expression of IL-12p40 homodimer. PLoS Pathog 2018;14(4):e1007001.
[5] Xiahou Z, Wang X, Shen J, et al. NMI and IFP35 serve as proinflammatory DAMPs during cellular infection and injury. Nat Commun 2017;8(1):950. doi: https://doi.org/10.1038/s41467-017-00930-9.
[6] Jing X, Yao Y, Wu D, et al. IFP35 family proteins promote neuroinflammation and multiple sclerosis. PNAS 2021. 118(32).10.1073/pnas.2102642118.
[7] Mao X, Wu D, Xu N, et al. The danger signal interferon-induced protein 35 (IFP35) mediates acetaminophen-induced liver injury. Biochem Biophys Res Commun 2022;621:25–31. doi: https://doi.org/10.1016/j.bbrc.2022.06.086.
[8] Zhang L, Zhu H, Li Y, et al. The role of IFI35 in lupus nephritis and related mechanisms. Mod Rheumatol 2017;27(6):1010–8. doi: https://doi.org/10.1080/14397595.2016.1270387.
[9] Yu Y, Xu N, Cheng Q, et al. IFP35 as a promising biomarker and therapeutic target for the syndromes induced by SARS-CoV-2 or influenza virus. Cell Rep 2021;37(12):. doi: https://doi.org/10.1016/j.celrep.2021.110126110126.
[10] Jiang X, Stockwell BR, Conrad M. Ferroptosis: mechanisms, biology and role in disease. Nat Rev Mol Cell Biol 2021;22(4):266–82. doi: https://doi.org/10.1038/s41580-020-00324-8.
[11] Jiang L, Kon N, Li T, et al. Ferroptosis as a p53-mediated activity during tumour suppression. Nature 2015;520(7545):57–62. doi: https://doi.org/10.1038/nature14344.
[12] Mahoney-Sánchez L, Bouchaoui H, Ayton S, et al. Ferroptosis and its potential role in the physiopathology of Parkinson's Disease. Prog Neurobiol 2021. 196 101890.10.1016/j.pneurobio.2020.101890.
[13] Linkermann A, Skouta R, Himmerkus N, et al. Synchronized renal tubular cell death involves ferroptosis. PNAS 2014;111(47):16836–41. doi: https://doi.org/10.1073/pnas.1415518111.
[14] Li P, Jiang M, Li K, et al. Glutathione peroxidase 4-regulated neutrophil ferroptosis induces systemic autoimmunity. Nat Immunol 2021;22 (9):1107–17. doi: https://doi.org/10.1038/s41590-021-00993-3.
[15] Li W, Feng G, Gauthier JM, et al. Ferroptotic cell death and TLR4/Trif signaling initiate neutrophil recruitment after heart transplantation. J Clin Invest 2019;129(6):2293–304. doi: https://doi.org/10.1172/jci126428.
[16] Amaral EP, Costa DL, Namasivayam S, et al. A major role for ferroptosis in Mycobacterium tuberculosis-induced cell death and tissue necrosis. J Exp Med 2019;216(3):556–70. doi: https://doi.org/10.1084/jem.20181776.
[17] Dar HH, Tyurina YY, Mikulska-Ruminska K, et al. Pseudomonas aeruginosa utilizes host polyunsaturated phosphatidylethanolamines to trigger theft-

Fig 6. IFP35 promotes Nrf2 degradation by enhancing K48-linked ubiquitination. (a) BMDMs were infected with SA (MOI = 200) for 3 h, and then were fixed and immunostained with Nrf2 and IFP35 antibodies. (b) HEK293T cells were transiently transfected with HA-IFP35 and Flag-Nrf2 for 24 h and then were infected with SA (MOI = 30) for 3 h. Cells were fixed and immunostained with anti-Flag and anti-HA antibodies. (c-d) HEK293T cells were transiently transfected with HA-IFP35 and Flag-Nrf2 or the control plasmid, as indicated. Cell lysates were subjected to IP with anti-HA (c) or anti-Flag (d) antibody, followed by IB analysis with anti-HA or anti-Flag antibody. Proteins in whole cell lysates were used as positive control (input). (e) HEK293T cells were transiently transfected with an HA-IFP35 plasmid or a control plasmid, together with a Flag-Nrf2 plasmid for 24 h and then treated with 10 μM CHX for various times. IB images of Nrf2 in cell lysates were shown. (f) HEK293T cells were transfected with a Flag-Nrf2 plasmid, together with an increasing number of HA-IFP35 plasmids (0, 0.5, 1, or 2 μg), and then treated with MG132 (10 μM) for 3 h, IB analysis of the cell lysates was shown. (g) HEK293T cells transfected with a Flag-Nrf2 plasmid and an HA-IFP35 plasmid and then treated with MG132 (10 μM) or chloroquine (100 μM) for 3 h, IB analysis of cell lysates from cell lysates was shown. (h-i) HEK293T cells were transiently co-transfected with Myc-ubiquitin (Ub) (h) or Myc-K48 (i), together with HA-IFP35, and Flag-Nrf2 for 24 h, and then treated with MG132 (10 μM) for 3 h. Cell lysates were subjected to IP with an anti-Flag antibody. (j-k) HEK293T cells were transiently co-transfected with Flag-Keap1, together with HA-IFP35, as indicated. Cell lysates were subjected to IP with anti-HA (j) or anti-Flag (k) antibody, followed by IB analysis with anti-HA or anti-Flag antibody. Proteins in whole cell lysates were used as positive control (input). (l) HEK293T cells were transiently transfected with an HA-IFP35 plasmid or a control plasmid, together with a Flag-Keap1 plasmid for 24 h, IB images of Keap1 in cell lysates were shown.

ferroptosis in bronchial epithelium. J Clin Invest 2018;128(10):4639–53. doi: https://doi.org/10.1172/jci99490.
[18] Ousingsawat J, Schreiber R, Gulbins E, et al. P. aeruginosa Induced Lipid Peroxidation Causes Ferroptotic Cell Death in Airways. Cell Physiol Biochem 2021;55(5). pp. 590–604.10.33594/000000437.
[19] Ma R, Fang L, Chen L, et al. Ferroptotic stress promotes macrophages against intracellular bacteria. Theranostics 2022;12(5):2266–89. doi: https://doi.org/10.7150/thno.66663.
[20] Anandhan A, Dodson M, Schmidlin CJ, et al. Breakdown of an Ironclad Defense System: The Critical Role of NRF2 in Mediating Ferroptosis. Cell Chem Biol 2020;27(4):436–47. doi: https://doi.org/10.1016/j.chembiol.2020.03.011.
[21] Anandhan A, Dodson M, Shakya A, et al. NRF2 controls iron homeostasis and ferroptosis through HERC2 and VAMP8. Sci Adv 2023;9(5). eade9585.10.1126/sciadv.ade9585.
[22] Chan JY, Kwong M. Impaired expression of glutathione synthetic enzyme genes in mice with targeted deletion of the Nrf2 basic-leucine zipper protein. BBA 2000;1517(1):19–26. doi: https://doi.org/10.1016/s0167-4781(00)00238-4.
[23] Qiang Z, Dong H, Xia Y, et al. Nrf2 and STAT3 Alleviates Ferroptosis-Mediated IIR-ALI by Regulating SLC7A11. Oxid Med Cell Longev 2020. 2020 5146982.10.1155/2020/5146982.
[24] Dong H, Qiang Z, Chai D, et al. Nrf2 inhibits ferroptosis and protects against acute lung injury due to intestinal ischemia reperfusion via regulating SLC7A11 and HO-1. Aging (Albany NY) 2020;12(13):12943–59. doi: https://doi.org/10.18632/aging.103378.
[25] Li S, Zheng L, Zhang J, et al. Inhibition of ferroptosis by up-regulating Nrf2 delayed the progression of diabetic nephropathy. Free Radic Biol Med 2021;162:435–49. doi: https://doi.org/10.1016/j.freeradbiomed.2020.10.323.
[26] Pan W, Zhu S, Qu K, et al. The DNA Methylcytosine Dioxygenase Tet2 Sustains Immunosuppressive Function of Tumor-Infiltrating Myeloid Cells to Promote Melanoma Progression. Immunity 2017;47(2):284–297.e5. doi: https://doi.org/10.1016/j.immuni.2017.07.020.
[27] Ouyang W, Liu C, Pan Y, et al. SHP2 deficiency promotes *Staphylococcus aureus* pneumonia following influenza infection. Cell Prolif 2020;53(1):e12721.
[28] Sun Y, Chen P, Zhai B, et al. The emerging role of ferroptosis in inflammation. Biomed Pharmacother 2020. 127 110108.10.1016/j.biopha.2020.110108.
[29] Lee J, Jang J, Park SM, et al. An Update on the Role of Nrf2 in Respiratory Disease: Molecular Mechanisms and Therapeutic Approaches. Int J Mol Sci 2021. 22(16).10.3390/ijms22168406.
[30] Heaton SM, Borg NA, Dixit VM. Ubiquitin in the activation and attenuation of innate antiviral immunity. J Exp Med 2016;213(1):1–13. doi: https://doi.org/10.1084/jem.20151531.
[31] Hu Y, Wang B, Yi K, et al. IFI35 is involved in the regulation of the radiosensitivity of colorectal cancer cells. Cancer Cell Int 2021;21(1):290. doi: https://doi.org/10.1186/s12935-021-01997-7.
[32] Chai D, Shi SY, Sobhani N, et al. IFI35 Promotes Renal Cancer Progression by Inhibiting pSTAT1/pSTAT6-Dependent Autophagy. Cancers (Basel) 2022. 14 (12).10.3390/cancers14122861.
[33] Chen X, Kang R, Kroemer G, et al. Ferroptosis in infection, inflammation, and immunity. J Exp Med 2021. 218(6).10.1084/jem.20210518.
[34] Kang R, Zeng L, Zhu S, et al. Lipid Peroxidation Drives Gasdermin D-Mediated Pyroptosis in Lethal Polymicrobial Sepsis. Cell Host Microbe 2018;24 (1):97–108.e4. doi: https://doi.org/10.1016/j.chom.2018.05.009.
[35] Kitur K, Parker D, Nieto P, et al. Toxin-induced necroptosis is a major mechanism of *Staphylococcus aureus* lung damage. PLoS Pathog 2015;11(4): e1004820.
[36] Loboda A, Damulewicz M, Pyza E, et al. Role of Nrf2/HO-1 system in development, oxidative stress response and diseases: an evolutionarily conserved mechanism. Cell Mol Life Sci 2016;73(17):3221–47. doi: https://doi.org/10.1007/s00018-016-2223-0.
[37] Dodson M, Castro-Portuguez R, Zhang DD. NRF2 plays a critical role in mitigating lipid peroxidation and ferroptosis. Redox Biol. (2019) 23 101107.10.1016/j.redox.2019.101107.
[38] Cuadrado A, Rojo AI, Wells G, et al. Therapeutic targeting of the NRF2 and KEAP1 partnership in chronic diseases. Nat Rev Drug Discov 2019;18 (4):295–317. doi: https://doi.org/10.1038/s41573-018-0008-x.
[39] Das A, Dinh PX, Panda D, et al. Interferon-inducible protein IFI35 negatively regulates RIG-I antiviral signaling and supports vesicular stomatitis virus replication. J Virol 2014;88(6):3103–13. doi: https://doi.org/10.1128/jvi.03202-13.